International Journal of Archaeology
2025; 13(2): 141-151
http://www.sciencepublishinggroup.com/j/ija
doi: 10.11648/j.ija.20251302.11
ISSN: 2330-7587 (Print); ISSN: 2330-7595 (Online)

An Exquisitely Fine Paint Brush for the Turin Shroud's Body Image

James. C. Porter*

Department of Physics and Astronomy, Eastern Michigan University, Ypsilanti, USA

Email address:
jporter@emich.edu (James. C. Porter)
*Corresponding author

To cite this article:
James. C. Porter. (2025). An Exquisitely Fine Paint Brush for the Turin Shroud's Body Image. *International Journal of Archaeology, 13*(2), 141-151. https://doi.org/10.11648/j.ija.20251302.11

Received: 13 May 2025; **Accepted:** 11 June 2025; **Published:** 14 July 2025

Abstract: The Shroud's body image is a monochromatic half-tone made from a huge number of short, straw yellow discolorations. These discolorations donot penetrate the trheads oreven all the way through the fibers which make up the threads. They appear only on a thin outer layer of the fibers, the fiber primary cell walls. In this work we show that the radioactive isotope rubidium 87 is found in linen fiber's primary cell walls in sufficient concentrations to initiate yellowing *should a large proportion undergo beta decay*. This kind of nuclear decay involves the emission of an anti-neutrino which escapes, so that the electron which is produced concurrently can have a variety of kinetic energies and can be launched in a variety of directions. We argue that radiation damage from electron irradiation could have produced uniform yellowing of the fiber primary cell walls and have quenched ultra-violet fluorescence, both characteristics of the Shroud's body image. Recent developements in the theory of quantum foundations point to the existance of a world, indistinguishable from ours and occupying our same spactime, in which the image was, with certainty, created by ^{87}Rb decays.

Keywords: Turin Shroud, Body Image, Rubidium 87, Beta Decay, Quantum Foundations

1. Introduction

The Turin Shroud is a 4.4 meter by 1.1 meter length of fine linen kept in the Cathedral of Saint John the Baptist in Turin Italy. It is one of the most important religious relics in the world, however its authenticity remains a topic of debate among anthropologists, scientists, and theologians. The present work does not address this issue, but rather focuses on the origin of the Shroud's body image. In this work the Shroud's *microimage* is defined as what was seen through the microscope during the STURP (Shroud of Turin Research Project) in 1978. The apposite *macro image* is what is seen upon stepping away from the microscope: a faint straw yellow halftone superimposed on the pale yellow of the antique linen. The next section describes features of the Shroud's microimage that comport with the rubidium hypothesis.

2. The Shroud's Microimage

The Shroud's threads are spun from an average of two hundred flaxen fibers [1] two to five centimeters long [2] and ranging in diameter from ten to twenty microns [1] (ten to twenty thousandths of a millimeter) an order of magnitude thinner than a human hair. The microimage is the product of fiber discolorations up to 300 microns in length and up to three deep at points where fibers cross the crowns of parent threads [1]. Discolorations are superficial with respect to fibers as well as threads in that discolorations reach no deeper than the fiber *primary cell walls*.

Figure 1 shows the primary cell wall of a fiber of average diameter in the flax stem and finished linen.

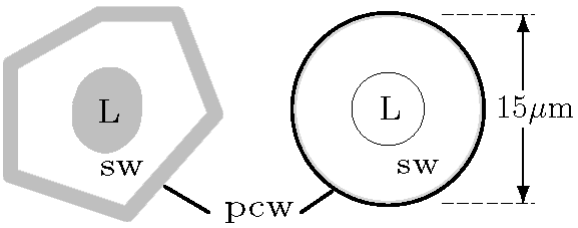

Figure 1. *A fiber cross section in the stem (left) and linen (right).*

In the flax stem, fiber primary cell walls, pcw, are eighty percent cytoplasmic water by weight [3], the rest being pectins, cellulose and hemicelluloses [4], surrounding the more rigid α-cellulose secondary walls, sw, [5]. In finished linen, drying reduces the primary wall water content to around six percent [6] and the primary wall thickness to just a fifth of a micron [4]. The lumen, L, is emptied and fulling has rounded the in-stem polygonal cross section.

In Figure 2 pointillistic features, dots and small strokes discoloring a warp thread, are pictured. Thread locations have been chosen to approximate those in a Mark Evans 100X photomicrograph, published in a 10 cm by 15 cm format on glossy paper [7], of a 1.5 square millimeter area. Here the Shroud was likely stretched a few millimeters above the corpus nose bridge [8], during the image formation process [9]. Warp threads, running parallel to the midline of the corpus, are horizontal and weft threads, w, are vertical. The linen is a 3/1 twill, so that the warp thread bearing the circled area surmounts three weft threads before bending downward to pass under a fourth. Linen threads are usually spun by twisting constituent fibers in the clockwise sense. This chirality aligns with the natural twist of the cellulose fibrils [10] found in the fiber secondary walls. The Shroud's threads, however, have been spun in the counterclockwise sense. The appearances of the weft, proceeding upward and to the left in Figure 2, rather than to the right as usual, partner with this counterclockwise chirality to give a smooth surface [11].

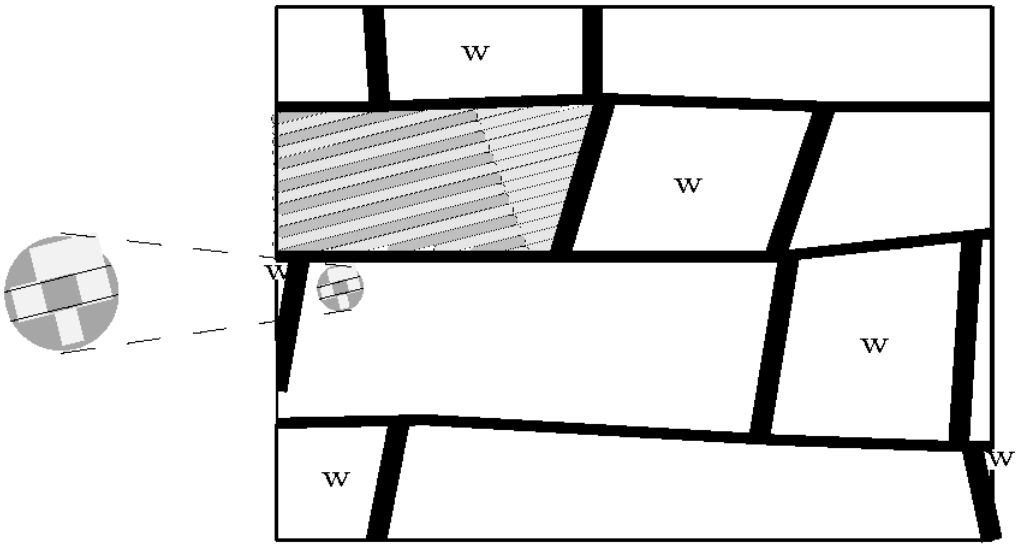

Figure 2. *Warp and weft threads above the corpus nose bridge.*

Focus stacking software [12] was not available to STURP researchers in 1978 and, with a depth of field of just 7 microns at 100X, only the area illustrated on one of the warp threads in the Mark Evans photomicrograph is resolved sufficiently to make out the approximate locations and 10 micron diameters of the fibers.

Beyound its mimicking of thread locations and its marking the location, (circled) of a rare, isolated 10 micron discolortion, Figure 2 bears no direct relation to the Mark Evans photomicrograph. Instead it illustrates, employing 20 micron fibers, properties of the discolortions found generally throughout the Shroud. These are first, *striations*, fibers discolored a straw yellow (dark gray in Figure 2) alternating with the pale yellow fibers of the background linen (light gray) and second, an absence of discolorations from areas where threads bend or dip [11]. Here discolorations are absent to the right of the inclined dotted line where a warp thread bends downward to pass under the weft.

The remainder of this work introduces an origination hypothesis that comports with these details of the microimage. This is discoloration via the decays of rubidium 87, a radioactive isotope that is concentrated in the primary cell walls of linen fibers. The following sections cover rubidium's abundance in plants and in flax fiber primary cell walls. Constraints imposed by fiber curvature vis-à-vis the straight line paths of rubidium's decay electrons and the observed uniform hue of discolorations are discussed qualitatively with quantitative considerations relegated to an appendix.

3. Rubidium in Plants and in the Shroud

Although not incorporated into the structure of cellulose, potassium is an essential plant nutrient. Rubidium, potassium's heavier congener, is also readily absorbed and is present in ordinary soils in the ratio of one rubidium atom to 202 atoms of potassium [13]. Because potassium 40, the radioactive component of potassium, makes up just 0.012 percent of environmental potassium, while 28 percent of rubidium is the radioactive 87 isotope, concentrations of $^{87}Rb^{+}$ ions in plant cytoplasmic water are eleven times greater than those of $^{40}K^{+}$. The minimum concentration of potassium cations required for plant growth has been estimated to be between 100 and 200 millimoles per liter [14] (i.e., at least $6 \cdot 10^{19}$ ions per gram). Accordingly a gram of cytoplasmic water in the flax stem may be expected to contain at least $3 \cdot 10^{17}$ rubidium ions.

As Figure 1 suggests, the potassium and rubidium ions, originally present in water that makes up four fifths of the primary wall's in-stem volume, are, in linen, packed into about one fifth of that volume, increasing their concentrations by a factor of four. Since approximately a quarter of natural rubidium is the 87 isotope, the expected concentration of $^{87}Rb^{+}$ in linen fiber primary cell walls is at least $3 \cdot 10^{17}$ ions per gram of primary cell wall material.

Rubidium concentrations in the Shroud are limited, according to a STURP X-ray fluorescence study [15], to less than about 0.5 micrograms per cm squared. However the mass of natural rubidium in the 25 to 30 milligrams of fiber that make up each square centimeter of the Shroud [11] is only about 0.3 μg per cm^2 because fiber secondary walls, constituting 94 percent of fiber mass, have only an 8 percent cytoplasmic water content [54] and consequently only about one fortieth of the rubidium concentrations found in the primary walls.

4. The Response of Cellulose to Radiation

The irradiation of cellulose with energetic electrons is known to result in the loss of the hydroxyl (-OH) groups ordinarily bonded to one of the five carbon atoms in each glycon ring of cellulose polymers [16]. This, together with the circumstance that hydroxyl groups are instrumental in triggering the fluorescence of polymer composites under ultraviolet irradiation [17], may explain why the Shroud's body image does not fluoresce under ultraviolet irradiation, this in contrast to the weak fluorescence of light scorches and of the background linen [18].

A suggestion, due to S. F. Pellicori and transmitted by Schwalbe and Rogers [11], linkes reduced crystallinity with the yellowing of cellulose. Two studies support this conjecture. In the first, a reduction in the crystallinity of cotton linters was found to be associated with increased transparency at the red end of the visible spectrum [19]. A second study, done by Saeman *et al.* in 1952 [20, 21], quantified the relation between irradiation with energetic electrons and reductions in crystallinity. Here cellulose from dried wood pulps and cotton linters was irradiated with a beam of 800 keV (kilo electron-Volt) electrons. At radiative doses exceeding 930 joules of absorbed energy per gram, depolymerization (i.e., reduced crystallinity) was observed and samples became "very fragile and slightly discolored" [20]. Scorching was avoided by accumulating doses in increments of 93 joules per gram with cooling periods between increments so that the maximum temperature rise in samples never exceeded 41°C.

Unlike the dry wood pulps studied by Saeman *et al.*, the Shroud's linen was probably moist during image formation. Assuming a water content of six percent by weight [6] and a temperature of 20°C, a total of 1080 joules of energy per gram of hemicellulose in fiber primary cell walls would have had to have been absorbed in order to evaporate the water [22], and then go on to produce discoloration.

5. Effects of Fiber Curvature

The short discoloration identified on Figure 2 is compatible with the rubidium hypothesis. Discolorations, however, much shorter than about 8 microns require that rubidium's decay electrons be emitted with so little energy that irradiations would not reach the 1080 joule per gram level. Rulling out very short isolated discolorations with certainty would probably require focus stacking photomicrography.

Discolorations longer than about 30 microns, if not created by overlapping shorter discolorations, are also rulled out. This is owing to three different kinds of constraints. First, energetic electrons travel in straight lines, at least until their kinetic energy falls below a few keV when collisions become important [23]. Second, electron tracks are not observed to have passed in quantity through fiber secondary cell walls [24]. And finally, surface fibers curve as they wind around a thread. If the parent thread lies flat, the abruptness with which fibers bend is a function only of the angle between the fiber where it crosses the thread crown and the thread's direction. For example, some published photomicrographs show an angles as large as 24 degrees [1]. In these cases surface fibers curve around the circumference of a circle whose radius equals six times that of their parent threads [25]. Fiber curvatures more abrupt than this are found to the right of the inclined dotted line in Figure 2 where fibers bend around circles whose radii may be only one or two times the warp thread radius. Here, discolorations even as short as 8 microns would require that rubidium's decay electrons pass in quantity through an adjacent secondary cell wall.

6. Producing Uniform Chromaticity

A deceptively simple property of the microimage's discolorations is their relatively uniform chromaticity, or hue, as one moves along a fiber [1]. Saeman *et al.*'s 800 keV beam

of energetic electrons facilitated spatially uniform irradiation because the beam's kinetic energy remained relatively constant as it transected samples. This is not the case for rubidium's decay electrons which loose energy at a rate approximately inversely proportional to the value of the energy itself [26] as they traverse primary cell wall material.

A protocol leading to the delivery of an approximately uniform radiative dose over a wide central portion of a fifteen micron long fiber segment is detailed in the appendix and summarized here with the help of Figure 3. The figure's top row represents the primary cell wall of the fiber segment as a thin-walled cylindrical shell. (The effects of fiber curvature are accounted for in the appendix but ignored here.) The geometry is simplified to a single dimension by treating the cylindrical shell as an assemblage of many narrow *strips*, each only as wide as the primary wall is thick. In Figure 3, a narrow gap in the shell marks where one of these strips has been removed and brought forward. In order to visualize electrons moving inside the strip, the strip's nearly square cross section is not shown to scale but instead is greatly enlarged.

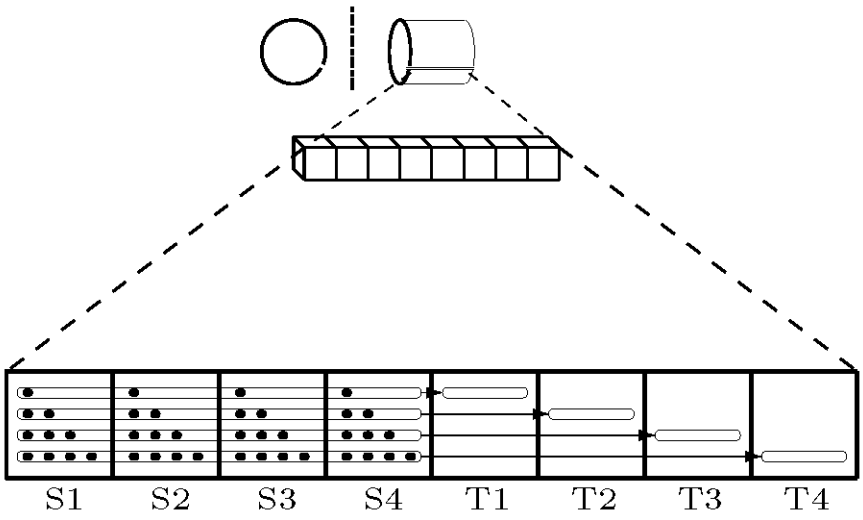

Figure 3. *A simplified protocol.*

Rubidium 87 decays are isotropic and can also produce electrons with a range of kinetic energies. Only a small fraction of possible decays emit an electron with a momentum and an energy within the range of values guaranteeing that the electron will stay inside a strip during the straight line portion of its travel. The rubidium hypothesis requires that the decays of *almost all* of the minimally expected number of ^{87}Rb nuclei present, $3 \cdot 10^{17}$ per gram of primary cell wall material, be part of this small fraction.

In order to maximize the radiative dose imparted to the hemicelluloses in the strips, electrons emitted in the left half of a strip are assumed to travel toward the right, while electrons emitted in the strip's right half travel toward the left. To parse electron emission energies, and thus electron travel lengths, with a view toward achieving uniformity of irradiation it is convenient to divide strips into a number of *bins*. Electrons are assumed to be moving from left to right in Figure 3, so that the four bins to the left of center strip, S_1 through S_4 are considered sources of electrons and bins to the right of center strip, T_1 through T_4, targets.

The bottom row of Figure 3 illustrates one way of assigning ten electrons from ^{87}Rb decays in each source bin to destinations in one or another of the four target bins. With a view toward maximizing uniformity of irradiation, it is convenient to summarize these assignments in the form of entries in a distribution list, $\{g_k\}$; $k = 1, 2, 3, 4$. In the example of Figure 3 this list would have four entries. The first, $g_1 = 0.1$, indicates that one tenth of the ten decay electrons present in each source bin are to be assigned kinetic energies at launch such that the straight line part of their motion will carry them into, but not beyond, the first target bin. Next, $g_2 = 0.2$, assigns two electrons from each source bin to the second target bin, and so on to $g_4 = 0.4$. The same distribution list is used again for a second round of irradiations where the roles of source and target are reversed and electrons travel toward the left.

In the appendix, a larger distribution list has twenty entries g_k; $k = 1, 2, \cdots 20$, where each entry, g_k, specifies the fraction of the approximately six thousand electrons, emitted from each of twenty source bins, that is to reach target bin T_k. It is reasonable to expect that g_k should increase with k, and trial and error shows that the rate of increase, assumed to be linear with k in the example of Figure 3, should be proportional to the fourth power of k in order to get approximate dose uniformity over a central portion of a strip. In Figure 4 the resulting radiative dose is plotted versus position along a 15 micron strip. (DR_i shows contributions from rightward moving electrons only.) Here i, numbering the bins, runs from one to 40.

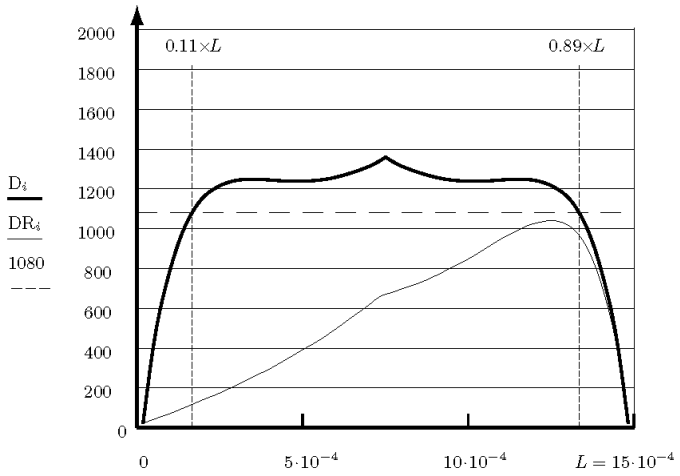

Figure 4. *Dose D_i (joules/gm) as a function of position (cm).*

Almost all of the microimage's discolorations are longer than fifteen microns and simple tip-to-tail replications of the profile in Figure 4 would lead to pale yellow notches interrupting straw yellow discolorations. Dosing in increments, separated by small spatial offsets parallel to a fiber's direction, can fill in these notches. An example, using 108 joule/gram dose increments and 1.5 micron offsets to produce a 300 micron discoloration, is described in the appendix.

With a distribution list in hand, the probability associated with the production of a 15 micron long discoloration can be found in terms of rubidium eighty seven's half-life and beta spectrum [27]. The result, under the assumption that the rubidium decays occurred over a three day period, is found in the appendix to be a jaw-dropping one part in ten raised to a power whose exponent is approximately 10^9. Accordingly, the origination of the Shroud's body image via ^{87}Rb decays seems to border on the miraculous. There are explanations for the Shroud's body image that do require miracles, processes for example that violate conservation of energy [28]. However here the conservation laws for energy, momentum, baryon number and so on are all satisfied.

7. Testing

A photomicrograph of what author Ray Rogers refers to as a "ghost" [7] was lifted from the Shroud on a sticky tape in 1978. In view of the fact that flax fiber primary cell walls are not cemented to secondary walls [29], Rogers' ghost is almost certainly the upper half of a fiber primary cell wall. Experimental verification that samples lifted from image areas of the Shroud are depleted with respect to their rubidium 87 content, relative to samples from non-image areas, would be decisive. Regrettably the combination of sub-nanogram sample sizes and interference on atomic mass number 87, due to the presence of strontium 87, rubidium's decay product and a component of rock dust, obviates testing at present. A review of the literature suggests that SIMS, (Secondary Ion Mass Spectrometry), can analyze samples this small but cannot distinguish between ^{87}Rb and ^{87}Sr because the fractional mass difference $(m_{s87_{\mathrm{Rb}}} - m_{s87_{\mathrm{Sr}}})/m_{s87_{\mathrm{Rb}}}$ is about one hundred times smaller than the mass sensitivity of the best quadrant mass spectrometers [30]. Because SIMS requires the maintenance of ultra-high vacuum throughout the measurement process, chemical separation as in ICP-MS/MS [31], cannot be used.

Not all testing need be deferred. The following section assumes that, should colorimetry measurements be made on linen irradiated at a level somewhere between one and two thousand joules of beta energy per gram and artificially aged [32], results will be found to comport with spectrophotometric data collected on the Turin Shroud in 1978 [33].

8. Discussion

Attempts to explain the Shroud's body image have posited a variety of mechanisms that allow information about the physiognomy of the corpus to shape the image. The rubidium hypothesis takes a different path. It relies on a peculiarity of quantum mechanics to make the provocative assertion that there exists a world, contemporaneous and coexistent with ours, in which the Shroud's body image *was created* by ^{87}Rb decays. This assertion follows from the "many worlds" interpretation of quantum mechanics. ("Many worlds" is a linguistic tag suggested by physicist Bryce DeWitt [34] as descriptive of Hugh Everett III's contribution to quantum foundations [35] in his 1957 PhD thesis [36, 37].) Not all physicists interested in quantum foundations are proponents of many worlds [38]. For example Roger Penrose, in his book *The Emperor's New Mind*, hopes that an eventual synthesis of quantum mechanics with general relativity will suggest an alternative [39].

A widely viewed U-tube video [40] makes it convenient to introduce many worlds ideas via the Schrödinger's cat paradox [41]. This animates a thought experiment designed to illustrate quantum "wierdness". The eponymous cat is isolated from the external environment inside a box along with a radioactive atomic nucleus which would poison the cat, should it decay before the box is opened. If the cat's time in the box equals the half-life of the radioactive nucleus there is a fifty percent probability for each outcome. Many worlds absolves nature from the need to choose between equally likely alternatives by asserting that the two incompatible outcomes are *both realized but in different worlds*. The world that hosted the observer who put the cat in the box has "split" or "branched" into two separate worlds by the time the box is opened and the cat observed. Neither one, of the two resultant observers, senses this for the reason that there is no communication between worlds in which differing quantum possibilities are realized, even though they occupy the same physical spacetime [42]. It can be argued [40] that this remarkable assertion, that an event on the scale of an atomic nucleus causes the entire universe to split into two universes, one with an observer and a dead cat and the other with an observer and a live cat, is a consequence of the peculiar nature of quantum mechanics as encapsulated in

its foundational relation, the Schrodinger wave equation [43].

Now consider these ideas in reference to the Shroud. Suppose that the radioactive nucleus in the box is rubidium 87. It is positioned near a sensor that can detect the presence of a decay electron and release the poison. In this case the possibility of a dead cat is almost zero. The cat would have to be in the box for longer than the age of the earth, (the half-life of the ^{87}Rb nucleus is $5 \cdot 10^{10}$ years [27]) to get to a fifty-fifty split. Does this mean that the world, when the box is opened after only a few days, invariably turns out to be one where the cat is alive? The answer is no; there is still a world with a surprised observer and a dead cat. Splits that are associated with greatly differing probabilities will have greatly differing energy contents, a "wide" part with almost all of the energy and a "narrow" part with only a tiny bit of the original energy. This possibility is illustrated in Sean Carroll's book *Something Deeply Hidden* [44].

Suppose that the sensor, the poison and the cat be replaced by a length of fine linen, the box by a tomb. Opening will almost always occur in a world where rubidium decays have not produced an image on the linen. Still there are worlds in which the linen will be seen to bear an image because some excessively large number of decays have taken place. These latter worlds are all super narrow, in terms of their energy content, but huge in number because rubidium decays have the potential to create a huge variety of images. In at least one of these worlds the linen bears an image indistinguishable from that on the Shroud of Turin.

Acknowledgments

The author thanks Drs. J. B. Ross and B. F. Muller for helpful discussions.

Conflicts of Interest

The author declares no conflicts of interest.

Appendix

Appendix I: Introduction

An initial section describes how the effect of mild fiber curvature can be simulated by a reduction in the percentage of ^{87}Rb nuclei that undergo decay by a factor derived from an average fiber radius of curvature. In the second section of the appendix a one dimensional treatment based on an empirical stopping power relation for electrons [26]. The relative paucity of decay electrons in this case necessitates the use of a discrete form of this stopping relation. A final section estimates the probability associated with the discoloration of a 15 micron segment of fiber.

Appendix II: Strips as One Dimensional Objects; Accounting for Curvature

Under the assumption that fiber curvature, as measured by the radius of an osculating circle [25], is never smaller than six thread radii, a 15 micron segment of fiber will subtend at most one degree of arc and the geometry of its primary cell wall will approximate that of a right circular cylinder of length $L = 0.0015$ cm. Sliced laterally, unrolled, flattened, and finally cut into thin *strips*, the primary wall can be treated in a one dimensional approximation.

For convenience the width of the strips t is assumed to be the same as their thickness $t = 0.2$ microns [4]. The number of such strips per segment is approximately $\pi\, d/t$, where $d = 15 \cdot 10^{-4}$ cm is the average fiber diameter. Strips are further considered to be subdivided into forty equally sized *bins* each of length $L/40$, with $N = 20$ bins on either side of the strip's center. Assuming that the density of primary cell walls is $\rho = 1.5$ grams per cc and with a spatially uniform distribution of ^{87}Rb$^+$ ions of $3.0 \cdot 10^{17}$ per gram, there will be $3.0 \cdot 10^{17} \times \rho\, t^2\, L/2N = 6750$ ^{87}Rb$^+$ ions per bin. Larger bins (smaller N) are possible but diminish the uniformity of the radiative dose that can be achieved. On the other hand, because bins hold only whole numbers of ^{87}Rb$^+$ ions and absorb only whole numbers of decay electrons, non-physical fluctuations in dosage become evident when N exceeds several hundred. Bins are identified by the locations of their centers, $\{x_i\}$, along an x-axis commencing at the strip's left end so that $x_i = (2i-1)(L/4N)$; for $i = 1,\, 2, \cdots 2N$. Bins left of center are located at $x = x_j$ for $j = 1,\, 2 \cdots N$, and bins right of center are located at $x = x_k$, for $k = N+1,\, N+2, \cdots 2N$.

The condition that dosage reductions, due to the disqualifications from radioactive decay necessary to avoid damage to secondary cell walls, should be small is that

$$C_{j,k} \equiv (x_k - x_j)^2/(8\, t\, \rho_c) \ll 1;\; j = 1,\, 2, \cdots N;\quad k = N+1,\, N+2, \cdots 2N, \tag{A-1}$$

where ρ_c is the strip's radius of curvature. Figure A1 shows a strip that has a latteral surface coplainar with the osculating circle. The dotted lines enclose an allowed set of electron trajectories and $C_{j,k}$ gives a disqualified fraction $\overline{\text{cb}}/\overline{\text{ab}}$ of about 0.1, a ten percent disqualification, if one takes $\rho_c \approx 6$ thread radii as representative of an average over the Shroud. The geometry leading to Eq. (A-1) is illustrated in Figure A1 where the strip's radius of curvature has been reduceded to 3.5 thread radii in order to better display the geometry. Ratios $\overline{\text{ab}}/(x_{40} - x_1)/\rho_c$=1/3/4 were used to construct Figure A1, in as much as this set of ratios leads to the disqualification of the same percentage of rubidium 87 decays, about 20 percent, as does the actual set of ratios in this case, 0.04/3/100, and is far easier to compactly illustrate.

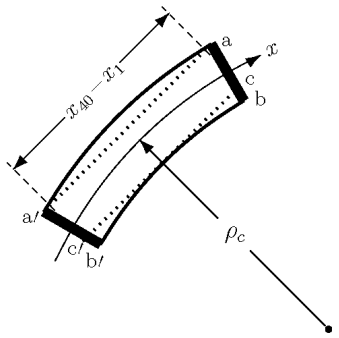

Figure A1. *A strip near the crown of its parent fiber.*

Appendix III: Creating Uniform Chromaticity

Irradiations are calculated in two stages: first bins left of center strip are taken to be sources of ^{87}Rb decay electrons, that then travel through their strip toward target bins to the right of the strip's center. Following this, the roles of source and target bins are interchanged with decay electrons traveling toward the left and the resulting radiative doses added. Decay electrons travel along straight line paths between source and target [23], deviating from their linear trajectories only when within their target bin where their kinetic energy will fall below a few keV and collisions randomize their motion.

Radiation dosages absorbed by bins at $x = x_i$, for $i > j$ and $i < k$, satisfy an empirical stopping power relation [26], that expresses the proportionality of the negative of the spatial gradient of an electron's kinetic energy at the center of a bin, (i.e., the energy that the electron imparts to the hemicelluloses in the bin divided by the bin width $L/2N$), to the value of the electron kinetic energy there, the latter raised to a power whose exponent is a negative eight tenths. The stopping power relation is valid for that part of the motion where straight line travel prevails, i.e., during travel from source to target bin where the electron's kinetic energy exceeds a few keV [26]. For definiteness 3 keV is used for this cutoff.

The stopping relation is

$$\frac{E(x_i - L/4N) - E(x_i + L/4N)}{L/2N} = \frac{K}{E(x_i)^{4/5}}\,;\, 1 \le j < i < k \le 2N, \tag{A-2}$$

for $E(x_i) \ge 3$ keV. Here the proportionality constant K is independent of the index i. $E(x_i)$ satisfies end conditions at $i = j$ and $i = k$ respectively as follows,

$$E(x_j) = 1400(x_k - x_j)^{5/9};\ \text{and}\ E(x_k) = 3, \tag{A-3}$$

where Eq. (A-3) gives the launch energy $E(x_j)$ in terms of the range $(x_k - x_j)$ for electrons exceeding 10 keV in a medium of density $\rho = 1.5$ grams per cc [45] and for electrons with energies between 3 keVS and 10 keV interpolated from Fig. 3-3 in reference [46].

A solution of Eq. (A-2) to first order in powers of

$$\lambda \equiv (L/(x_k - x_j))/2N, \tag{A-4}$$

that satisfies Eqs.(A-3) is given by

$$E(x_i) = 1400\left(x_k - x_i + \left(\frac{3}{1400}\right)^{9/5}\frac{x_i - x_j}{x_k - x_j}\right)^{5/9}. \tag{A-5}$$

Substituting Eq. (A-5) on the left in Eq. (A-2), the negative spatial gradient of a decay electron's kinetic energy, in keV per cm, becomes

$$\frac{E(x_i - L/4N) - E(x_i + L/4N)}{L/2N} = \frac{1400\,\mathcal{E}_{j,i,k}}{1.8\,(x_k - x_j)^{4/9}}\,;\, 1 \le j < i < k \le 2N, \tag{A-6}$$

where the factor

$$\mathcal{E}_{j,i,k} \equiv \frac{1 - \left(\frac{3}{1400}\right)^{9/5}\frac{1}{x_k - x_j}}{\left(1 + \left(\frac{3}{1400}\right)^{9/5}\frac{x_i - x_j}{(x_k - x_i)(x_k - x_j)}\right)^{4/9}}$$

reflects the cutoff in Eq. (A-2) at 3 keV. Dividing by $\rho\, t^2$, the line density along the strip in grams per cm, and multiplying by $1.6 \cdot 10^{-16}$ joules per keV on the right in Eq. (A-6) gives the radiative dose absorbed by strip hemicelluloses in bin i, in joules per gram, imparted by an electron traveling from bin j to bin k.

Adding contributions from all electrons traveling from left to right entails the inclusion of, an as yet undetermined distribution list g_k, a multiplicative factor that gives the fraction of electrons emitted in source bins with a launch energy sufficient to produce a linear trajectory into, but not beyond, the k-th target bin. A choice that leads to a relatively uniform distribution of irradiation over a centered 78 percent of a strip's length is given by

$$g_k = \left(\frac{k - N}{N}\right)^5 - \left(\frac{k - N - 1}{N}\right)^5, \tag{A-7}$$

where g_k approximates a normalized quartic monomial on the interval [L/2,L]. The sum over $k = N{+}!, \cdots 2N$ of g_k equals unity as required, and that the average length of the straight line portion of an electron's path is two thirds of the strip length, or 10 microns.

Summing in Eq. (A-6) over $j = 1, \cdots N$ and $k = N + 1, \cdots 2N$ gives the radiative dose DR_i, in joules per gram, absorbed by the hemicelluloses in bin i that is delivered by electrons moving toward the right:

$$DR_i = \begin{cases} \displaystyle\sum_{k=N+1}^{2N} \left[\frac{1400}{1.8} \cdot \frac{1.6 \cdot 10^{-16}}{\rho t^2 (x_k - x_i)^{4/9}} \right. \\ \qquad \left. \times \displaystyle\sum_{j=1}^{i} (1 - C_{j,k}) \mathcal{E}_{j,i,k}\, n_k \right]; \qquad \text{if } 2 \le i \le N, \\ \displaystyle\sum_{k=i+1}^{2N} \left[\frac{1400}{1.8} \cdot \frac{1.6 \cdot 10^{-16}}{\rho t^2 (x_k - x_i)^{4/9}} \right. \\ \qquad \left. \times \displaystyle\sum_{j=1}^{N} (1 - C_{j,k}) \mathcal{E}_{j,i,k}\, n_k \right]; \qquad \text{if } N+1 \le i \le 2N-1, \end{cases} \tag{A-8}$$

where

$$n_k \equiv 3 \cdot 10^{17} (\rho\, L\, t^2 / 2N) g_k \tag{A-9}$$

is the number of electrons whose kinetic energy falls below 3 keV in the k-th target bin. The parameter λ, Eq. (A-4), is relatively large for values of the index k not much larger than N, with the implication that the solution Eq. (A-5) is poor in this region. Here this doesn't matter, since g_k is nearly zero for $k \lessapprox 30$ and is sharply peaked as k approaches 40. Thus Eq. (A-8) should give acceptable results.

Adding contributions from electrons moving left, $DL_i = DR_{2N+1-i}$ to get $D_i = DR_i + DL_i$ yields an approximately uniform dose of radiation over a central 78 percent of the strip, with nearly linear fall-offs at either end as shown in Figure A2.

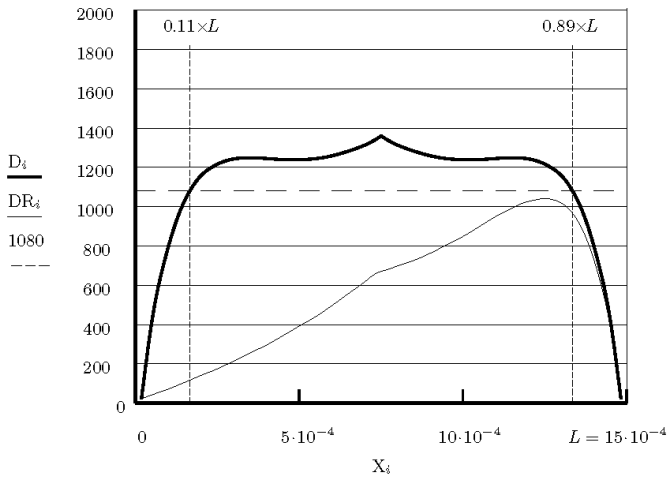

Figure A2. *Dose (j/gm) as a function of position (cm).*

Longer discolorations, for example one 300 microns in length, could have resulted from the irradiation of twenty one 15 micron lengths articulated "tip to tail" around the circumference of a circle of radius ρ_c, dosing first with the targeted decay of just a ten percent tranche of the ^{87}Rb nuclei present in the first twenty 15 micron lengths and then offsetting the next ten percent tranche of decays along the circle's circumference by 1.5 microns. Continuing with eight additional offsets and eight subsequent irradiations results in a central 0.03 cm of a 0.033 cm length of primary cell wall having been dosed with 1080 joules per gram. Nearly linear fall-offs 15 microns long are produced at either end.

Appendix IV: Probability

Finally, consider the probability associated with the irradiation of a single 15 micron length of primary cell wall. Like all beta decays, the beta decay of the ^{87}Rb nucleus is stochastic; the probability per second for a decay is time invariant. The decay is also isotropic, so there is a finite probability that the ^{87}Rb nucleus's decay electron will be launched sufficiently parallel to the axis of the nucleus's surrounding primary cell wall so that nearly all of its kinetic energy remains inside the primary wall. Finally, the fact that the probability density as a function of electron launch energy is known for the ^{87}Rb nucleus, allows the calculation of the probability associated with rubidium decays that end their journeys down strip at locations contributing to the absorption of a spatially uniform radiative dose.

The half-life of ^{87}Rb is $5 \cdot 10^{10}$ years so that the probability that a given rubidium 87 nucleus inside a strip of primary wall material will decay over a nominal three day period is $0.693\,(3/365)/(5 \cdot 10^{10}) \approx 1.1 \cdot 10^{-13}$. (Radiation damage didn't accrue over some very short time period as fibers were not scorched.)

The probability for an emission direction, sufficiently parallel to the strip so that an electron emitted at $x = x_j$ will not exit the strip before it reaches the location $x = x_k$, is approximately the ratio of solid angles

$$\left(\frac{t}{x_k - x_j} \right)^2 \Big/ 4\pi. \tag{A-10}$$

Next the probability density for ^{87}Rb decays can be obtained from Flynn *et al.* [27] and [47]Eisberg. For launch energies between approximately 0 keV and 40 keV, this is

$$KE_{j,k}\left(2.16\cdot 10^{-2}-2.60\cdot 10^{-4}KE_{j,k}+1.55\cdot 10^{-6}(KE_{j,k})^2\right)^2, \tag{A-11}$$

where $KE_{j,k} = 1400(x_k - x_j)^{5/9}$ is the kinetic energy at emission associated with travel between bins j and k, in a medium of density 1.5 gm/cc, (c.f., Eq. (A-3)).

Finally, the joint probability, $p_{j,k}$, for the passage of an electron from the source bin j to target bin k is the product of a timely rubidium decay, $1.1\cdot 10^{-13}$, with the factors given in expressions (A-10), (A-11) and (A-12) below,

$$\left(1400(x_k-x_j+\frac{L}{4N})^{5/9}-1400(x_k-x_j-\frac{L}{4N})^{5/9}\right), \tag{A-12}$$

where (A-12) gives the difference in launch energy corresponding to a difference in travel distance of $L/2N$, the bin width.

Since the number of decaying ^{87}Rb nuclei in each of twenty source bins is approximately ninety percent of 6750, or 6075, assuming that ten percent of the ^{87}Rb nuclei present do not decay as mentioned in conjunction with Eq. (A-1), the joint probability for electron travel between all N source bins into all N target bins is

$$P_{\text{left to right}}=\prod_{j=1}^{N}\prod_{k=N+1}^{2N}(p_{j,k})^{6075\,g_k}=10^{-2.4\cdot 10^6}. \tag{A-13}$$

The square of the probability in Eq. (A-13) gives the joint probability for electron motion in both directions through a strip, $10^{-4.8\cdot 10^6}$ and the probability for the formation of a 15 micron long segment of primary wall this, raised to a power whose exponent is the number of strips in a segment $\pi\, d/t$,

$$P_{15\ \mu\text{ m segment}}=10^{-4.8\cdot 10^6\times\pi\cdot d/t}=10^{-1.1\cdot 10^9}. \tag{A-14}$$

References

[1] G. Fanti, J. A. Botella, P. Di Lazzaro, T. Heimburger, R. Schneider and N. Svensson. Microscopic and Macroscopic Characteristics of the Shroud of Turin Image Superficiality. *J. Imaging Sci. Technol.*, 54(4): 040201-040201-8, Jul–Aug 2010. https://doi.org/10.2353/J.ImagingSci. Technol.2010.54.4.04020

[2] H. L. Bos and A. M. Donald. In situ ESEM study of the deformation of elementary flax fibres. *Journal of Materials Science*, 34:3029–3034, 1999.

[3] S. P. Hardegree. Derivation of plant cell wall water content by examination of the water-holding capacity of membrane-disrupted tissues. *J. Exp. Bot.* 219: 1099–1104, 1989.

[4] C. Goudenhooft, A. Bourmaud, and C. Baley. Flax (Linum usitatissimum L.) Fibers for Composite Reinforcement: Exploring the Link Between Plant Growth, Cell Walls Development, and Fiber Properties. *Front. Plant Sci.*, 10(411): 1–23, 2019. https://doi.org/10.3389/fpis.2019.00411

[5] A. S. Crafts, H. B. Currier and C. R. Stocking. *Water in the Physiology of Plants*. Chronica Botanica Co., Waltham Mass., 1949.

[6] T. Xie, C. A. S. Hill, Z. Jalaludin, S. F. Curling, R. D. Anandjiwala, A. F. Norton and G. Newman. The dynamic water vapour sorption behaviour of natural fibres and kinetic analysis using the parallel exponential kinetics model. *J. Mater Sci.*, 46: 479–489, 2011. https://doi.org/10.1007/s10853–010–4935–0

[7] R. N. Rogers. *A Chemist's Perspective on the Shroud of Turin*. Barrie M. Schwortz, www.Shroud.com, ISBN=978–0–6152–3928–6, July 2008.

[8] J. P. Jackson, E. J. Jumper and B. Mottern. The Three Dimensional Image on Jesus' Burial Cloth. In *Proceedings of the 1977 United States Conference of Research on the Shroud of Turin*, Edited by K. E. Stevenson. Holy Shroud Guild, March 1977.

[9] J. P. Jackson, E. J. Jumper and W. Ercoline. Correlation of image intensity on the Turin Shroud with the 3-D structure of a human body shape. *Appl. Opt.*, 23(14): 2244–2270, July 1984.

[10] K. Nyholm, P. Ander, G. Bardage and G. Daniel. Dislocations in Pulp fibers - their origin, characteristics and importance - a review. *Nord. Pulp Pap. Res. J.*, 4: 376–384, 2001.

[11] L. A. Schwalbe and R. N. Rogers. Physics and Chemistry of the Shroud of Turin, A Summary of the 1978 Investigation. *Anal. Chim. Acta*, 135: 3–49, 1982.

[12] J. Cremona. *Extreme Close-Up Photography and Focus Stacking*. The Crowood Press Ltd. Wiltshire, SN8 2HR, UK., 2014.

[13] R.O. Hanson, R. D. Vidao and P. R. Stout. Radioisotopes in Soils: Physical-Chemical Composition. In *Radioisotopes in the Biosphere*, Edited by R. S. Caldecott and L. A. Snyder. University of Minnesota Center for Continuation Study of the Gereral Extension division, 1960.

[14] R. A. Leigh and R. G. Wyn Jones. A Hypothesis Relaating Critical Potassium Concentrations For Growth To The Distributioin And Functions Of This Ion In The Plant Cell. *New Phytol.*, 97: 1–13, 1984.

[15] R. A. Moris, L. A. Schwalbe and J. R. London. X-Ray Fluorescence Investigation of the Shroud of Turin. *X-Ray Spectrom.*, 9(2): 40–47, 1980.

[16] L. Klarhöfer, W. Viöl and W. Maus-Friedrichs. Electron spectrosasma treated lignin and cellulose. *Holzforschung*, 64: 331–336, 2010.

[17] R. Tian, J. Zhong, C. Lu and X. Duana. Hydroxyl-triggered fluorescene for locaion of inorganic materials in polymer-matrix composites. *Chem. Sci.*, 9(1): 218–222, 2018.

[18] S. F. Pellicori. Spectral properties of the Shroud of Turin. *Applied Optics*, 19(12): 1913–1920, 1980.

[19] R. T. O'Conner. Analysis of Chemically Modified Cotton. In *High Polymers Volume V, Part IV, Cellulose and Cellulose Derivatives*, Edited by N. M. Bikales and L. Segal. Wiley-Interscience. 1971.

[20] J. f. Saeman, M. A. Millett and E. J. Lawton. Effect of High-Energy Cathode Rays on Cellulose. *Ind. and Eng. Chem.*, 44(12): 2848–2852, 1952.

[21] National Bureau of Standards. Section 2.19 in *Radiological Monitoring Methods and Insuruments*. U.S. Department of Commerce, 1952.

[22] L. Pauling. *College Chemistry*. W. H. Freeman and Company, 1955.

[23] H. S. Bethe and M. E. Rose. The Multiple Scattering of Electrons. *Proc. Am. Phil. Soc.*, 78: 573–585, 1938.

[24] R. N. Rogers. The Shroud of Turin Radiation Effects, Aging and Image Formation. https://www.shroud.com/pdfs/rogers8.pdf (accessed June 19, 2019), 2005.

[25] G. A. Korn and T. M. Korn. *Mathematical Handbook for Scientists and Engineers*. 2nd ed. McGraw-Hill 1968.

[26] D. C. Joy and S. Luo. An Empirical Stopping Power Relationship for Low-Energy Electrons. *Scanning*, 11: 176–180, 1989.

[27] K. F. Flynn and L. E. Glendenin. Half-Life and Beta Spectrum of Rb^{87}. *Phys. Rev.*, 116(3): 744–748, 1959.

[28] J. P. Jackson. The Fall-through Hypothesis. In *History, Science, Theology, and the Shroud: Symposium Proceedings, St. Louis Missouri*, 1991.

[29] K. Esau. *Plant Anatomy*, 2nd ed. Wiley and Sons Inc. 1958.

[30] H. Hutter. Dynamic Secondary Ion Mass Spectrometry (SIMS). In *Surface and thin Film Analysis: Principles, Instrumentation, Applications*, Edited by H. Bubert and H. Jenett. Wiley-VCH Verlag, GmbH. 2002. https://doi.org/10.1002/3527600167

[31] C. T. Laureijs, L. A. Coogan and J. Spence. A high throughput Rb-Sr dating method using solution tandem ICP-MS/MS ($^{87}Sr/^{86}Sr$) and standard addition calibration ICP-MS (Rb/Sr). *MethodsX* 8:101309–101309–14, 2021. https://doi.org/10.1016/j.mex.2021.101309

[32] L. Garlaschelli. Life-size reproduction of the Shroud of Turin and its Image. *J. Imaging Sci. Technol.*, 54(4): 040301-040301-14, 2010. https://doi.org/10.2352/J.imagingSci.Technol. 2010.54.4.040301

[33] L. Schwalbe and S. Pillicori. Analysis of Photoelectric Colorimetry and Fluoremetry of the Turin Shroud. *International Journal of Archaeology*, 11(1): 1–8, 2023. http://doi.org/10.11648/j.ija.20231101.11

[34] B. S. DeWitt. Quantum Mechanics and reality. *Phys. Today*, 23(9): 30–35, 1970. https://doi.org/10.1063/1.3022331

[35] M. J. W. Hall. Can Classical Worlds Emerge from Parallel Quantum Universes? https://physics.aps.org/articles/v17/155 (accessed May 6, 2025).

[36] H. Everett III. "Relative State" formulation of quantum mechanics. *Rev. Mod. Phys.*, 29(454): 454–462, 1957. https://doi.org/10.1103/RevModPhys.29.454

[37] H. Everett III. The Theory of the Universal Wave Function. In *The Many Worlds Interpretation of Quantum Mechanics*, Edited by B. S. DeWitt and N. Graham. Princeton University Press. 1973.

[38] M. Schirber. Quantum Milestoned, 1957: Sprouting Parallel Universes. https://physics.aps.org/articles/v18/83 (accessed May 6, 2025) 2025.

[39] R. Penrose. *The Emperor's New Mind*. Oxford University Press, Oxford, UK., 1999.

[40] Veritasium. Parallel Worlds Probably Exist: Here's Why. https:/www.youtube.com/watch?v=kTXTPe3wahc (accessed May 6,2021) 2020.

[41] E. Schrödinger. The present situation in quantum mechanics. In *Quantum Theory and Measurement*, Edited by J. A. Wheeler and W. H. Zurek. Princeton University Press, Princeton NJ., 1983.

[42] P. Strasberg, T. T. Reinhard and J. Schindler. First Principles Numerical Demonstration of Emergent Decoherent Histories. *Phys. Rev. X*, 14(4): 041027(17), 2024. https://doi.org/10.1103/Phys.RevX.14.041027

[43] E. Schrödinger. An Undulatory theory of the mechanics of atoms and molecules. *The Physicsl Review*, 28(6): 1049–1069, 1926.

[44] S. Carroll. *Something Deeply Hidden* Penguin Random House LLC. 2019.

[45] L. Katz and A. S. Penfold. Range-Energy Relations for Electrons and the Determination of Beta-Ray End-Point Energies by Absorption. *Reviews of Modern Physics*, 24(1): 28–44, 1952.

[46] P. Pianetta. Low-Energy Electron Ranges in Matter. In *Center for X-Ray Optics X-Ray Data Booklet*, Edited by D. Vaughan. Lawrence Berkeley Laboratory, University of California. 1985.

[47] R. M. Eisberg. Chapter 16, Section 11 in *Fundamentals of Modern Physics*, Wiley and Sons, 1961.